Nanoscale Research Letters

NANO EXPRESS Open Access

High-Performance $CsPbI_2Br$ Perovskite Solar Cells with Zinc and Manganese Doping

Ubaid Khan[1,2], Yu Zhinong[1*], Abbas Ahmad Khan[1,2], Almas Zulfiqar[2] and Naeem Ullah[3]

Abstract

Photovoltaic performances of $CsPbI_2Br$ solar cells are still lower than those of hybrid inorganic–organic perovskite solar cells, and researchers are exploring ways to improve their efficiencies. Due to its higher thermal stability in comparison with the generally studied hybrid inorganic–organic perovskites, all-inorganic $CsPbI_2Br$ has recently attracted great attention. By utilizing the combination of $MnCl_2$ and $ZnCl_2$ particles doping to modulate film growth, it is found that $MnCl_2$ and $ZnCl_2$ particles infiltrate into the holes of the $CsPbI_2Br$ lattice through the growth procedure, leading to suppressed nucleation and reduced growth rate. The combination assists to achieve higher $CsPbI_2Br$ crystalline grains for increased J_{sc} as high as 15.66 mA cm^{-2} and FF as large as 73.37%. It is indicated that a specific combination of $ZnCl_2$-$MnCl_2$ doping can fundamentally improve the film surface morphology, reduce trap density, and suppress the recombination of carriers. Consequently, power conversion efficiency (PCE) is significantly improved from 13.47 to 14.15% compared with the reference device without doping.

Keywords: Perovskite solar cell, Defect density, Stability, $CsPbI_2Br$, $ZnCl_2$-$MnCl_2$ doping

Introduction

Hybrid organic–inorganic perovskites have aroused great concerns because of their excellent electronic and optical properties [1–7] such as high mobility of the charge carriers and tunable band gap [8–11]. Notably, the power conversion efficiency (PCE) of perovskite-based organic–inorganic hybrid solar cells has improved from 3.8 to 23.3% through the cation exchange [12–17]. There are still challenges to overcome all environmental degradation [18]. Up to now, the cesium lead halide perovskite solar cells have been researched by many groups [19–22]. The large band gap of $CsPbBr_3$ is about 2.3 eV, which is too large to absorb long-wavelength lights [23, 24]. The $CsPbI_3$ has a low band gap of 1.73 eV, but it degrades rapidly from black phase to yellow phase at ambient temperature [25, 26]. $CsPbI_2Br$ perovskite shows a desirable band gap of 1.91 eV and is stable in the black phase in ambient air [19, 20]. It is demonstrated that the size of microcrystalline grain is a key factor for increasing the efficiency of solar cell. [27–30]. It appears that the grain boundaries in the surface of perovskite film suppress the recombination of the charges in their trap states [31]. Meanwhile, grain boundaries can provoke external states near the edge of the valence band which will impede the spread of the hole [32]. Therefore, it is desirable that the $CsPbI_2Br$ has a huge particle size and a low trap charge density [33]. For this purpose, the doping of impurities was explored extensively by incorporating several ions into the host lattice to modulate the performance of the film [34]. For example, by incorporating potassium into $CsPbI_2Br$, these large $CsPbI_2Br$ crystallites could be obtained to improve the formation of charge carriers and the better charge transport increases PCE [35]. Chu et al. used KCl as an additive material to obtain uniform and dense $MAPbI_3$ perovskite films with large grain-size nanocrystals [22]. Liu et al. reported that the addition of Mn^{2+} with a certain amount could significantly improve the crystalline grain size and achieve superior solar cell performance [36]. All-inorganic $CsPbI_2Br$ has recently attracted great attention due to its higher thermal stability in comparison with the generally studied hybrid inorganic–organic perovskites. In the paper, it is indicated that a specific combination of $ZnCl_2$-$MnCl_2$ doping can fundamentally improve the film surface morphology, reduce trap density, and suppress the recombination

* Correspondence: znyu@bit.edu.cn
[1]School of Optics and Photonics, Beijing Engineering Research Center of Mixed Reality and Advanced Display, Beijing Institute of Technology, Beijing 100081, China
Full list of author information is available at the end of the article

of carriers. Consequently, PCE is significantly improved from 13.47 to 14.15% compared with the reference device without doping. To the best of our knowledge, the PCE of 14.15% is among the best performance of $CsPbI_2Br$ perovskite solar cells.

Results and Discussion

We prepared 1.0 M using solution CsBr together with equal stoichiometric PbI_2 in mixed solvents of DMF and DMSO as the precursor solution. Through a one-step spin-coating method, a 350-nm film (measured by profilometer) was obtained after being annealed at 150 °C. To study the effect of additive on the film morphology and the device performance, we incorporated different contents of $ZnCl_2$-$MnCl_2$ (0%, 0.25%, and 0.50%) molar ratio, marked by $CsPbI_2Br$-0%, $CsPbI_2Br$-0.25%, and $CsPbI_2Br$-0.50%, respectively, into the $CsPbI_2Br$ precursor solution.

Figure 1a–c shows the top-view of $CsPbI_2Br$ films with different levels of $ZnCl_2$-$MnCl_2$. It can be seen that when the combination of $ZnCl_2$-$MnCl_2$ content is less than 0.25%, the $CsPbI_2Br$ film becomes more uniform and compact with the increase of the $ZnCl_2$-$MnCl_2$ content. In addition, there are almost no pin holes in the $CsPbI_2Br$-0.25% film, suggesting that the combination of $ZnCl_2$-$MnCl_2$ dopants is in favor of surface morphology of films. In the $CsPbI_2Br$-0.50%, however, small pin holes emerge in the film, which can create derivation paths and result in worse device performance.

Figure 2a shows the XRD patterns of the $CsPbI_2Br$ films doped using different $ZnCl_2$-$MnCl_2$ concentrations. The thicknesses of all the $CsPbI_2Br$ films are controlled to be 350 nm. Figure 2b shows the enlarged region of the (100) peak. It can be seen that the peak of the $CsPbI_2Br$-0.25% film shifts to a higher angle, indicating that the lattice constant is decreased. XPS analysis was performed to study the elemental composition and chemical state of the elements in the $CsPbI_2Br$-$ZnCl_2$-$MnCl_2$ films. Figure 2c–f shows the XPS spectra of all components with the exception of $ZnCl_2$ and $MnCl_2$. As appeared in Fig. 2c, the Cs 3d range determines two peaks at 724.4 eV and 739.8 eV, which are apportioned to Cs 3d 3/2 and Cs 3d 5/2 of Cs+ cations, respectively. Figure 2d–f demonstrates that Pb 4f, I 3d, and Br 3d peaks shift to higher binding energy, which indicates that some Zn and Mn particles may replace certain Pb atoms located in B-sites of the perovskite, and therefore, the chemical bonding between halides and lead have been changed due to the $ZnCl_2$-$MnCl_2$ doping [35]. This is consistent with the above XRD analysis.

The lightweight J–V curves of the cells based on the $CsPbI_2Br$-$ZnCl_2$-$MnCl_2$ films are shown in Fig. 3a, and the relevant photovoltaic parameters are recorded in Table 1. The $CsPbI_2Br$-0.25% device shows a champion PCE of 14.15%, with J_{sc} of 15.66 mA cm^{-2}, V_{oc} of 1.23 eV, and FF of 73.37%, which are totally higher than those of the $CsPbI_2Br$-0% device. We attribute this progress to enhanced film quality and reduced defects resulted from the $ZnCl_2$-$MnCl_2$ doping. External quantum efficiency (EQE) is done to verify the accuracy of J_{sc} completed from the J–V curve. As appeared in Fig. 3b, the EQE and interconnected J_{sc} of $CsPbI_2Br$-0.25% device are greater than those of the $CsPbI_2Br$-0% device. The interconnected J_{sc} of the $CsPbI_2Br$-0.25% device is 15.66 mA cm^{-2}, which is close to the J_{sc} of 14.86 mA cm^{-2} from the J–V bend. To research charge exchange properties of perovskite solar cells (PSCs), electrochemical impedance spectroscopy EIS spectra was completely abstracted as a function of voltage. The recombination resistance (R_{rec}) was extracted from the diameter of the semicircle in the Nyquist plots. Figure 3c shows that the R_{rec} of the $CsPbI_2Br$-0% and $CsPbI_2Br$-0.25% devices are 620 Ω and 1016 Ω, respectively. The much larger R_{rec} for the $CsPbI_2Br$-0.25% device originates from lower defect density, which indicates that charge recombination is effectively suppressed, leading to significantly improved V_{oc} and FF [37]. Figure 3d presents the typical J–V curves of the device with the best measured performance. Using the scanning directions of forward and reverse, the key parameters are summarized in the insert. It is noticeable that the device has very little hysteresis, as shown by the J–V curves.

Finally, we studied the long-term stability of the perovskite solar cells PSCs based on the $CsPbI_2Br$-0.25%

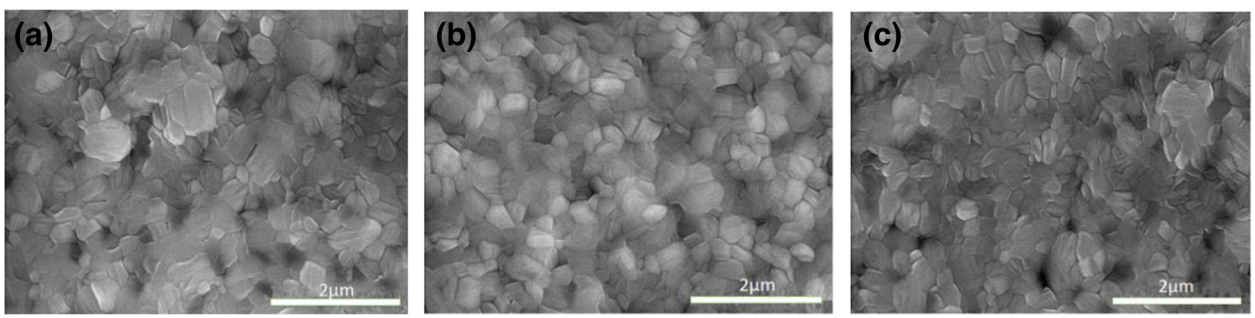

Fig. 1 The top-view SEM images of the $CsPbI_2Br$-$ZnCl_2$-$MnCl_2$ films. **a** $CsPbI_2Br$-0%. **b** $CsPbI_2Br$-0.25%. **c** $CsPbI_2Br$-0.50%

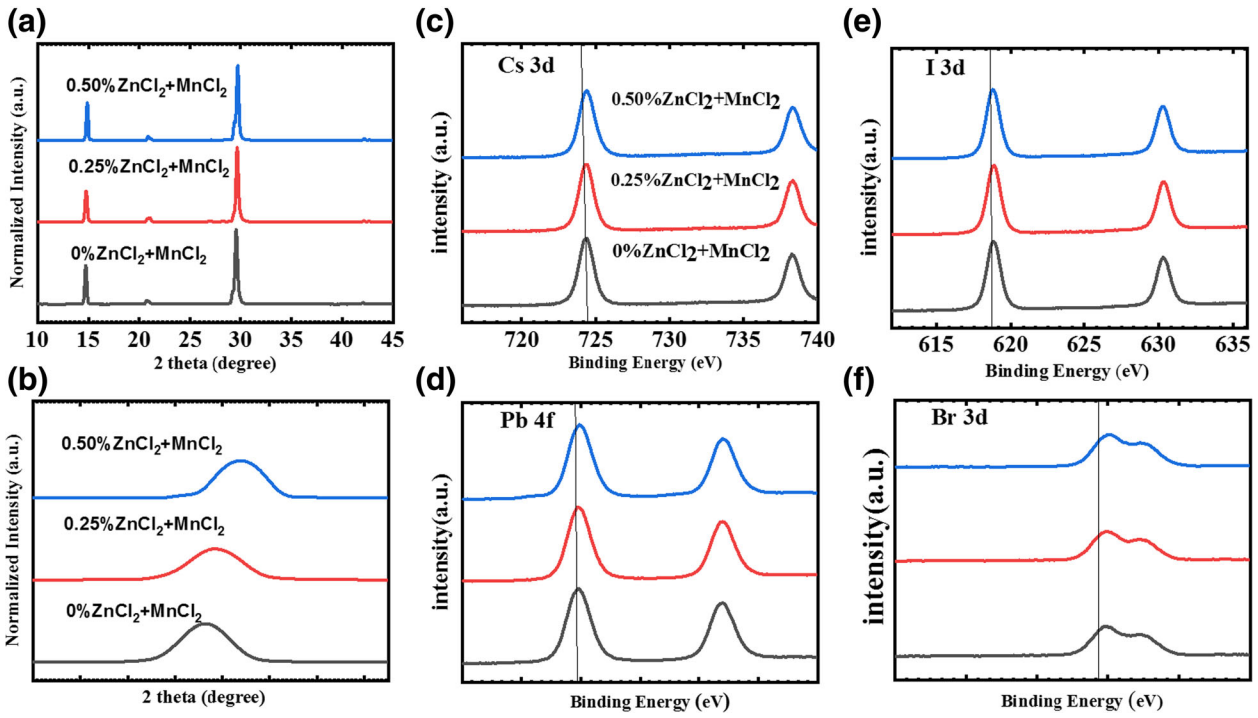

Fig. 2 X-Ray diffraction (XRD) patterns (**a**) and the enlarged region of (100) peaks (**b**) for the $CsPbI_2Br$-$ZnCl_2$-$MnCl_2$ films. XPS spectra of the $CsPbI_2Br$-$ZnCl_2$-$MnCl_2$ films for Cs 3d (**c**), Pb 4f (**d**), I 3d (**e**), and Br 3d (**f**)

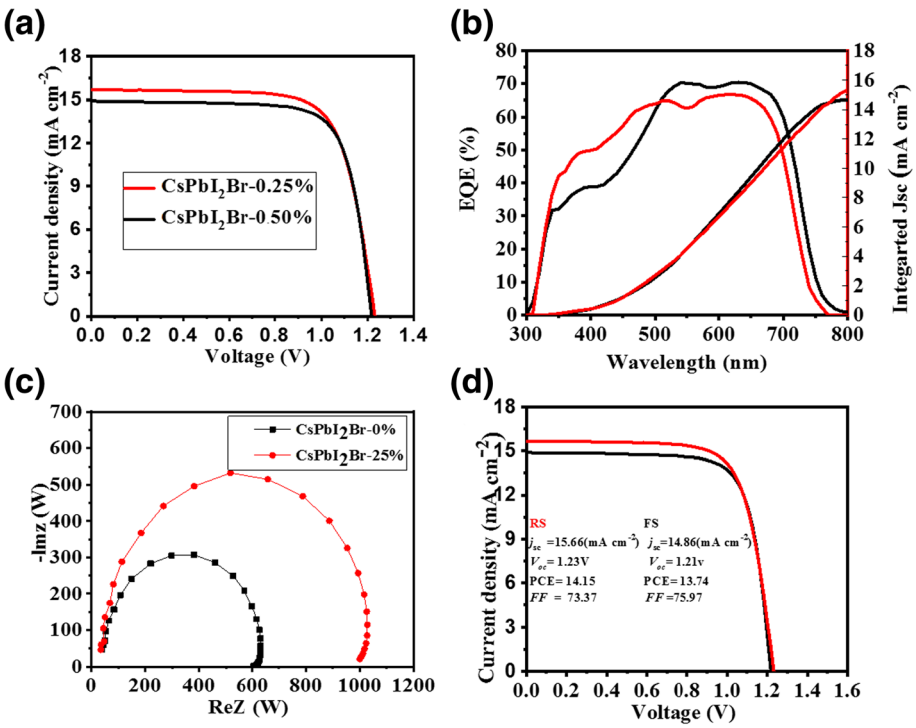

Fig. 3 Lightweight *J–V* curves of the solar cells based on the $CsPbI_2Br$-$ZnCl_2$-$MnCl_2$ films (**a**). EQE spectra and integrated J_{sc} of the solar cells based on the $CsPbI_2Br$-0.25% (red) and the $CsPbI_2Br$-0% (black) films (**b**). Nyquist plots (**c**). *J–V* characteristics under the directions of reverse and forward scanning (**d**)

Table 1 Comparison of the device parameters of the perovskite solar cells based on different $CsPbI_2Br$-$ZnCl_2$-$MnCl_2$ films

	PCE [%]	J_{sc} [mA cm^{-2}]	V_{oc} [V]	FF [%]
$CsPbI_2Br$-0.25% RS	14.15	15.66	1.23	73.37
$CsPbI_2Br$-0.25% FS	13.74	14.86	1.21	75.97
$CsPbI_2Br$-0%	13.01	14.21	1.24	73.64
$CsPbI_2Br$-0.50%	13.74	14.86	1.21	75.97
$CsPbI_2Br$-0.125%	12.62	13.6	1.27	73.0

film. The device was stored in a N_2 glove box (20 °C in the dark). Figure 4a shows the normalized J_{sc}, V_{oc}, FF, and PCE as a function of the storage time. During the first 3 days, J_{sc}, FF, and PCE all increase. This might be attributed to oxidation of spiro-OMeTAD by trace O_2 (300–400 ppm) in the glove box. After 30 days, the PCE maintains 87% of its initial value and V_{oc} keeps almost constant. We expect that these results will help the development of cesium lead halide perovskites for next-generation photovoltaic. The histogram of 30 devices' power conversion efficiency is shown in Fig. 4b, with statistics for photovoltaic parameters. Figure 4c shows the thermal stability of $CsPbI_2Br$-0.25% device tested by heating the device at 80 °C for 150 min in the glove box, and after heating, the PCE of device maintains 96% of its initial value and V_{oc} keeps almost constant. The absorption spectra of ultraviolet–visible (UV–vis) were carried out to observe the photo physical characteristics for the $CsPbI_2Br$-$ZnCl_2$-$MnCl_2$ films fabricated on glass substrate with a thickness of 70 nm. Figure 4d shows the absorption spectra of the $CsPbI_2Br$-0.25% film. The absorption intensity is almost the same for all the $CsPbI_2Br$-$ZnCl_2$-$MnCl_2$ films, and the absorption onset is around 600 nm. The above result suggests that the slight $ZnCl_2$-$MnCl_2$ doping hardly affects the band gap and the light absorption capacity of perovskite.

Experimental Section

Materials and Methods

Materials

The SnO_2 were bought from Alfa Aesar. CsBr, $ZnCl_2$, $MnCl_2$, (DMSO), and (DMF) were bought from Sigma-Aldrich. spiro-OMeTAD and PbI_2 were bought from Xi'an Polymer Light Technology Corp.

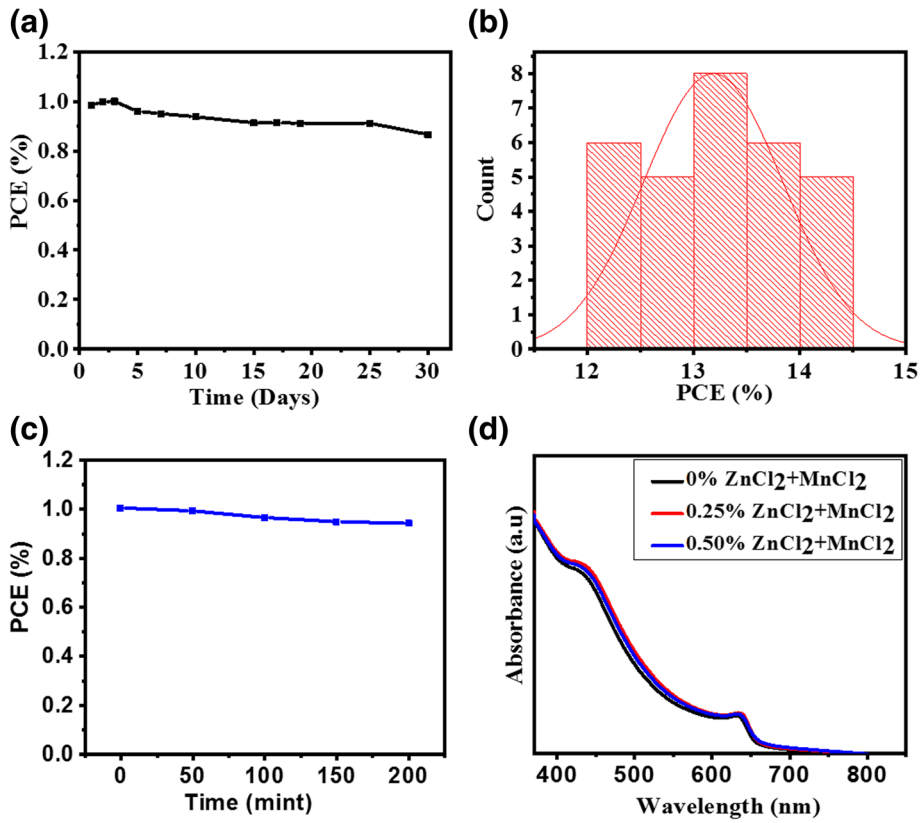

Fig. 4 Normalized V_{oc}, J_{sc}, FF, and PCE for the solar cell based on the $CsPbI_2Br$-0.25% film as a function of storage time (**a**). Histogram of power conversion efficiency values for 30 devices (**b**). Normalized PCE for the solar cell based on the $CsPbI_2Br$-0.25% film as a function of thermal treatment time (**c**). Absorption spectra (**d**)

Device Fabrication

Initially, the ITO glasses were successively cleaned by applying detergent, isopropyl alcohol, acetone solvents about 20 min, and deionized water. The process is also followed by removing the substances remain in the substrates through oxygen plasma processing approximately for 10 min. The SnO_2 were diluted in ultrapure water at a volume ratio of 1:6. Firstly, glass substrates were spin coated by SnO_2 layer at 3000 rpm for 40 s, and then were annealed at 150 °C for 30 min. To prepare a perovskite precursor, CsBr, PbI_2, $ZnCl_2$, and $MnCl_2$ were stoichiometrically dissolved in a mixed solvent of DMSO and DMF with a volume ratio of 1.4:1 to form a 1.0 M solution. The solution was filtered through a 0.22-μm pore PTFE filter, and then stirred at 70 °C for 2 h. The precursor solution was then spin coated on the SnO_2/ITO substrate firstly at 1000 rpm with accelerating rate of 1000 rpm for 12 s, after that at 5000 rpm with accelerating rate of 3000 rpm not more than 30 s. Then, 100 μL of chlorobenzene (CB) were distilled onto the rotating substrate during the second step spin-coating with the time of 10 s before the end of the process. Afterwards, the film was first annealed at 50 °C for 1 min and then at 150 °C for 5 min. An HTL film was prepared by spin-coating spiro-OMeTAD solution onto the formed $CsPbI_2Br$ film at 4000 rpm with accelerating rate of 3000 rpm for 30 s. The spiro-OMeTAD solution consisted of 72.3 mg Spiro-OMeTAD, 17.5 μL bis (trifluoro methane) sulfonamide lithium salt (Li-TFSI) stock solution (520 mg Li-TFSI in 1 mL acetonitrile), 28.8 μL 4-tertbutylpyridine, and 1 mL chlorobenzene. At the end, the Au film with a thickness of 80 nm was deposited through thermal evaporation.

Characterization

The Rigaku-2500 X-ray diffraction meter was used to measure the X-ray diffraction patterns. The top-view SEM images were attained using a scanning electron microscope (SEM, HITACH2100). Keithley 2420 was used to measure the solar cell *J–V* characteristics under AM 1.5 sunlight at an irradiance of 100 mW cm^{-2} provided by a solar simulator (Newport, Oriel Sol3A Class AAA, 94043A). The intensity of light was measured by monocrystalline silicon reference cell with a KG5 window (Newport, Oriel 91150). Impedance spectroscopy was measured by Zennium (Zahner). EQE was recorded using a Newport Oriel IQE-200 by a power source (Newport 300 W xenon lamp, 66920) with a monochromatic instrument (Newport Cornerstone 260). The device area is 0.044 cm^2.

Conclusions

In summary, we got inorganic $CsPbI_2Br$ solar cells by incorporating $ZnCl_2$-$MnCl_2$ into the $CsPbI_2Br$ precursor solution. When the $ZnCl_2$-$MnCl_2$ content achieves 0.25%, the device shows a champion PCE of 14.15%, with FF of 73.37%, J_{sc} of 15.66 mA cm^{-2}, and V_{oc} of 1.23 eV. The enhanced photovoltaic performance is associated to improved surface morphology, reduced trap density, and suppressed charge recombination. This work could guide fundamental researches in the Cesium lead halide perovskites and promote their potential applications for solar cell.

The Table of Contents Entry

A simple compositional engineering technique is used to improve the film quality and device performance. By incorporating $MnCl_2$+$ZnCl_2$ into the $CsPbI_2Br$ film, the $CsPbI_2Br$ perovskite solar cell attains an outstanding efficiency of 14.15% and good long-term stability. In addition, the fabrication process is highly reproducible and inexpensive.

Abbreviations

DMF: N,N-dimethylformamide; DMSO: Dimethyl sulfoxide; EQE: External quantum efficiency; SEM: Scanning electron microscope; XPS: X-ray photoelectron spectroscopy; XRD: X-ray diffraction

Acknowledgements

Special thanks to Professor Dr. Jizheng Wang for his valuable suggestions from, Institute of Chemistry, Chinese Academy of Sciences,

Funding

This research work were supported by the (NSFC) National Natural Science Foundation of China (Grant numbers No. 61675024, and No. 61874009).

Availability of Data and Materials

The results of this article are incorporated within the article datasets.

Authors' Contributions

UK fabricated the devices and performed the experiments. UK and AAK analyzed the data. YZ, AZ, and NU revised the manuscript. Finally, all authors approved the final manuscript to be submitted.

Competing Interests

The authors declare that they have no competing interests.

Publisher's Note

Author details

[1]School of Optics and Photonics, Beijing Engineering Research Center of Mixed Reality and Advanced Display, Beijing Institute of Technology, Beijing 100081, China. [2]Institute of Chemistry, Chinese Academy of Sciences, Beijing 100190, China. [3]School of Optics and Photonics, Beijing Institute of Technology, Beijing 100081, China.

Received: 4 January 2019 Accepted: 12 March 2019
Published online: 02 April 2019

References

1. Zhang T et al (2018) High speed and stable solution-processed triple cation perovskite photodetectors. In: Advanced Optical Materials, p 1701341
2. Liu D et al (2019) Improved stability of perovskite solar cells with enhanced moisture-resistant hole transport layers. Electrochim Acta 296:508–516
3. Ahmad W et al (2019) Physisorption of oxygen in SnO 2 nanoparticles for perovskite solar cells. IEEE Journal of Photovoltaics 9(1):200–206

4. Yang R et al (2019) To reveal grain boundary induced thermal instability of perovskite semiconductor thin films for photovoltaic devices. IEEE Journal of Photovoltaics 9(1):207–213
5. Manser JS et al (2016) Making and breaking of lead halide perovskites. Acc Chem Res 49(2):330–338
6. Xiao JW et al (2017) The emergence of the mixed perovskites and their applications as solar cells. Adv Energy Mater 7(20):1700491
7. Zhang T et al (2019) Low-temperature processed inorganic perovskites for flexible detectors with broadband Photoresponse. Nanoscale
8. Zhou H et al (2014) Interface engineering of highly efficient perovskite solar cells. Science 345(6196):542–546
9. Wei H et al (2016) Sensitive X-ray detectors made of methylammonium lead tribromide perovskite single crystals. Nat Photonics 10(5):333
10. Zhang Y et al (2017) Optimization of stable quasi-cubic FA x MA1–x PbI3 perovskite structure for solar cells with efficiency beyond 20%. ACS Energy Letters 2(4):802–806
11. Khan AA et al (2018) Solution processed trilayer structure for high-performance perovskite photodetector. Nanoscale Res Lett 13(1):399
12. Chen Q et al (2017) Ag-incorporated organic–inorganic perovskite films and planar heterojunction solar cells. Nano Lett 17(5):3231–3237
13. Zhang H et al (2017) SrCl2 derived perovskite facilitating a high efficiency of 16% in hole-conductor-free fully printable mesoscopic perovskite solar cells. Adv Mater 29(15):1606608
14. Wang Q et al (2016) Thin insulating tunneling contacts for efficient and water-resistant perovskite solar cells. Adv Mater 28(31):6734–6739
15. Weerasinghe HC et al (2015) Encapsulation for improving the lifetime of flexible perovskite solar cells. Nano Energy 18:118–125
16. D'innocenzo V et al (2014) Excitons versus free charges in organo-lead tri-halide perovskites. Nat Commun 5:3586
17. Zhang D et al (2015) Solution-phase synthesis of cesium lead halide perovskite nanowires. J Am Chem Soc 137(29):9230–9233
18. Petrus ML et al (2017) Capturing the sun: a review of the challenges and perspectives of perovskite solar cells. Adv Energy Mater 7(16):1700264
19. Beal RE et al (2016) Cesium lead halide perovskites with improved stability for tandem solar cells. The journal of physical chemistry letters 7(5):746–751
20. Sutton RJ et al (2016) Bandgap-tunable cesium lead halide perovskites with high thermal stability for efficient solar cells. Adv Energy Mater 6(8):1502458
21. Ma Q et al (2016) Hole transport layer free inorganic CsPbIBr2 perovskite solar cell by dual source thermal evaporation. Adv Energy Mater 6(7): 1502202
22. Lau CFJ et al (2017) Strontium-doped low-temperature-processed CsPbI2Br perovskite solar cells. ACS Energy Letters 2(10):2319–2325
23. Akkerman QA et al (2017) Strongly emissive perovskite nanocrystal inks for high-voltage solar cells. Nat Energy 2(2):16194
24. Zhou S, Tang R, Yin L (2017) Slow-photon-effect-induced photoelectrical-conversion efficiency enhancement for carbon-quantum-dot-sensitized inorganic CsPbBr3 inverse opal perovskite solar cells. Adv Mater 29(43):1703682
25. Swarnkar A et al (2016) Quantum dot–induced phase stabilization of α-CsPbI3 perovskite for high-efficiency photovoltaics. Science 354(6308):92–95
26. Zhang T et al (2017) Bication lead iodide 2D perovskite component to stabilize inorganic α-CsPbI3 perovskite phase for high-efficiency solar cells. Sci Adv 3(9):e1700841
27. Niezgoda JS et al (2017) Improved charge collection in highly efficient CsPbBrI2 solar cells with light-induced dealloying. ACS Energy Letters 2(5): 1043–1049
28. Zeng Q et al (2018) Polymer-passivated inorganic cesium lead mixed-halide perovskites for stable and efficient solar cells with high open-circuit voltage over 1.3 V. Adv Mater 30(9):1705393
29. Bi C et al (2015) Non-wetting surface-driven high-aspect-ratio crystalline grain growth for efficient hybrid perovskite solar cells. Nat Commun 6:7747
30. Xiao Z et al (2014) Solvent annealing of perovskite-induced crystal growth for photovoltaic-device efficiency enhancement. Adv Mater 26(37):6503–6509
31. Chen Q et al (2014) Controllable self-induced passivation of hybrid lead iodide perovskites toward high performance solar cells. Nano Lett 14(7): 4158–4163
32. Guo Y, Wang Q, Saidi WA (2017) Structural stabilities and electronic properties of high-angle grain boundaries in perovskite cesium lead halides. J Phys Chem C 121(3):1715–1722
33. Chen Z et al (2017) Thin single crystal perovskite solar cells to harvest below-bandgap light absorption. Nat Commun 8(1):1890
34. Swarnkar A, Mir WJ, Nag A (2018) Can B-site doping or alloying improve thermal-and phase-stability of all-inorganic CsPbX3 (X= Cl, Br, I) perovskites? ACS Energy Letters 3(2):286–289
35. Nam JK et al (2017) Potassium incorporation for enhanced performance and stability of fully inorganic cesium lead halide perovskite solar cells. Nano Lett 17(3):2028–2033
36. Bao Q et al (2009) Atomic-layer graphene as a saturable absorber for ultrafast pulsed lasers. Adv Funct Mater 19(19):3077–3083
37. Jiang J et al (2018) Polymer doping for high-efficiency perovskite solar cells with improved moisture stability. Adv Energy Mater 8(3):1701757